Japanese Journal of
Applied Physics

The Japan Society of Applied Physics

REGULAR PAPER

Buried annealed proton-exchanged waveguide in periodically-poled MgO:$LiTaO_3$ fabricated by surface-activated bonding for high-power wavelength conversion

To cite this article: Ryosuke Noro *et al* 2024 *Jpn. J. Appl. Phys.* **63** 062002

View the article online for updates and enhancements.

You may also like

- Going Beyond Sweep Voltammetry: Alternative Approaches in Search of the Elusive Electrochemical Stability of Polymer Electrolytes
Guiomar Hernández, Isabell L. Johansson, Alma Mathew et al.

- Nonlinear frequency conversion in semiconductor optical waveguides using birefringent, modal and quasi-phase-matching techniques
S Venugopal Rao, K Moutzouris and M Ebrahimzadeh

- Highly coherent mid-infrared wideband supercontinuum generation by a silica cladded silicon nitride core buried waveguide
Somen Adhikary, Dipankar Ghosh and Mousumi Basu

This content was downloaded from IP address 49.98.231.202 on 25/12/2025 at 03:48

Japanese Journal of Applied Physics **63**, 062002 (2024) **REGULAR PAPER**
https://doi.org/**10.35848/1347-4065/ad4c43**

Buried annealed proton-exchanged waveguide in periodically-poled MgO:$LiTaO_3$ fabricated by surface-activated bonding for high-power wavelength conversion

Ryosuke Noro[1*], Masahide Okazaki[2], Masahiro Uemukai[1], Tomoyuki Tanikawa[1], and Ryuji Katayama[1*]

[1]*Graduate School of Engineering, Osaka University, Suita, Osaka 565-0871, Japan*
[2]*Nikon Corporation, Tokyo 108-6290, Japan*

[*]E-mail: noro.r@qoe.eei.eng.osaka-u.ac.jp; katayama.ryuji@eei.eng.osaka-u.ac.jp

Received January 24, 2024; revised April 17, 2024; accepted May 14, 2024; published online June 10, 2024

Watt-class UV laser lights with symmetric spatial modes are suitable for high-resolution industrial applications. Channel waveguides with a guided mode of several ten microns diameter in MgO:$LiTaO_3$ enhance integration capability while avoiding photorefractive damages during high-power wavelength conversion. We focused on buried waveguides fabricated by proton exchange, surface-activated bonding (SAB), and proton diffusion processes in periodically-poled (PP) MgO:$LiTaO_3$. In this work, the mode profiles were simulated using the proton diffusion coefficients estimated by secondary ion mass spectrometry. Using the simulation results, the buried waveguides with a mode diameter larger than 30 μm were fabricated. By adopting designed PP structures, second harmonic generation (SHG) devices at a wavelength of 532 nm were fabricated. The nonlinear coupling coefficient was estimated to be 0.15 $W^{-1/2}$ cm^{-1}. Compared to the conventional annealed proton-exchanged waveguide SHG device without SAB, symmetric guided modes were obtained while maintaining the nonlinear coupling coefficient.
© 2024 The Japan Society of Applied Physics

1. Introduction

High-power UV lasers[1,2] are important light sources in various regions of industry, including laser direct imaging, material processing, semiconductor inspection, and laser cleaning.[3] In the laser direct imaging system, 350 nm band lasers are utilized to expose conventional i-line photoresists. Tens of 1 W laser beams, obtained by splitting a 10 W or higher power laser beam, can draw patterns on a whole area of a 300 mm wafer in ten seconds. Currently, 350 nm band lasers are realized using borate crystals by cascading second harmonic generation (SHG) and sum frequency generation (SFG) with a 1064 nm pump laser. A wavelength conversion with borate crystals utilizes birefringence phase matching.[2,4] Several tens watts laser light generation has been reported with a 100 W pump power since the borate crystals show a high optical damage threshold.[2,4,5] However, most of the borate crystals show hygroscopic properties,[5] leading increasing instability and maintenance costs. If 1 W UV laser beams are obtained by a 10 W pumping, high throughput and reasonable footprint multibeam laser direct imaging systems without complex beam splitting optical components can be realized. Single-beam laser direct imaging systems with the 1 W UV laser are also currently in demand for high-mix low-volume production. From the points of view of wavelength conversion efficiency and maintenance costs, the borate crystals are not suitable for the 1 W UV laser systems.

Ferroelectric crystals, such as MgO-doped congruent $LiNbO_3$ (MgO:CLN) and MgO-doped stoichiometric $LiTaO_3$ (MgO:SLT) have been widely used for wavelength conversion devices since they show a high optical nonlinearity and no hygroscopic properties.[6–16] Quasi-phase matching (QPM) is used for the various types of wavelength conversion, including the SHG for green light emission and the SFG for 350 nm band UV light emission, in the ferroelectric crystals. The photorefractive damage thresholds of 2 MW cm^{-2} of both MgO:CLN and MgO:SLT are one of the highest values in the ferroelectric crystals.[17] A nonlinear optical coefficient of MgO:CLN of 25.0 pm V^{-1} is higher than that of MgO:SLT of 13.8 pm V^{-1}.[6] However, MgO:CLN is difficult to apply to high-power uses due to its green induced infrared absorption (GRIIRA) under the high-power excitation.[13,18] On the other hand, a quite low level of GRIIRA has been reported in MgO:SLT crystals.[17,19,20] In actual high-power SHG, heat from both pump and SH light absorption saturates the SH power, and efficient thermal removal from the nonlinear crystals has been reported.[11,14,15] 10 W-class green SHG with a pump power of tens of watts has been achieved in bulk MgO:SLT crystals.[7–9] Additionally, its short absorption edge of 270 nm allows the crystals to generate 350 nm band UV lights. A 96 mW UV light generation with a wavelength of 355 nm has been realized by cascading a bulk SHG device and a bulk SFG device in MgO:SLT.[12]

In ferroelectric crystals, waveguide structures are utilized to enhance the conversion efficiency even for a low pump power wavelength conversion.[21–23] Specifically, annealed proton-exchanged (APE) waveguides with a guided mode diameter of several microns are widely used.[24–28] The APE waveguides have a graded refractive index profile and show low scattering loss.[25] For a high-power wavelength conversion, however, the power density of the lights tends to exceed the above photorefractive damage threshold. Thus, in order to obtain higher generated power, not only the increase of the pump power but also the enlargement of the guided mode diameter should be required to keep the pump power density close to the photorefractive damage threshold. In a recent study, we fabricated the enlarged APE waveguide with large mode diameters of 43 μm × 27 μm with a pump light at a wavelength of 1030 nm by extended annealing of 75 h.[16] However, the APE waveguides substantially possess an asymmetric refractive index profile, resulting in vertically asymmetric shapes of the guided mode. Asymmetricity of the UV light reduces the resolution of the laser direct imaging systems. Reverse proton exchanging (RPE) is one of the methods to mitigate the asymmetry of the refractive index profile.[29–31] The largest refractive index of the RPE waveguides is located inside the crystal, and the refractive index profile becomes close to a symmetrical shape.[30] However, enlarging the mode size of the RPE waveguides requires a

© 2024 The Japan Society of Applied Physics
All rights, including for text and data mining, AI training, and similar technologies, are reserved.

significantly longer fabrication time of about several times longer than that of APE waveguides with a large guided mode because the annealing time and the RPE time have to be extended to several hundreds of hours to ensure deep proton diffusion inside the crystal.

Another waveguide with a symmetric refractive index profile is buried APE waveguide using direct bonding techniques.[32] This waveguide is fabricated by direct bonding of the PE crystal and the non-PE crystal, followed by the annealing. Because protons can diffuse across the bonded interface during annealing, the refractive index profile becomes almost symmetrical in this method. Furthermore, the annealing time can remain within a realistic timeframe of 50–100 h when extending the refractive index profile for enlarging the guided mode size. To apply buried APE waveguide using direct bonding to wavelength conversion devices, the periodically-poled (PP) structures of both crystals must be aligned, otherwise the conversion efficiency will decrease.

To fabricate the buried APE waveguides with a large guided mode size, a diffusion coefficient of the protons in the crystals is one of the key parameters. According to our knowledge, the proton diffusion coefficient of the annealing in MgO:SLT has been estimated only in Ref. 28 using the mode size of the waveguide. However, the diffusion coefficient would not be accurate since the mode size in the APE waveguides is affected not only by diffusion depth. Moreover, the proton diffusion coefficient of the PE has not been reported. Therefore, in this paper, the proton diffusion coefficients of the PE and the annealing were estimated by secondary ion mass spectrometry (SIMS). Then, the guided mode profiles at various PE widths, PE times, and annealing times were simulated. Using the simulation results, the buried waveguides with the large guided mode were fabricated by direct bonding for symmetric pump and SH modes. Then, buried APE waveguides in PP MgO:SLT for a SHG at a wavelength of 532 nm were fabricated. The misalignment of the PP structures of both crystals was avoided by forming a uniform PP structure on one of the crystals and several sets of shifted PP structures on the other crystal. The SHG was demonstrated as a first step toward a high-power UV light source consisting of the SHG and SFG devices.

2. Device description and target mode diameters

Figure 1 illustrates a buried APE waveguide in PP MgO:SLT for high-power SHG. The period of the PP structure is 8.0 μm for the SHG with a pump wavelength of 1064 nm. The

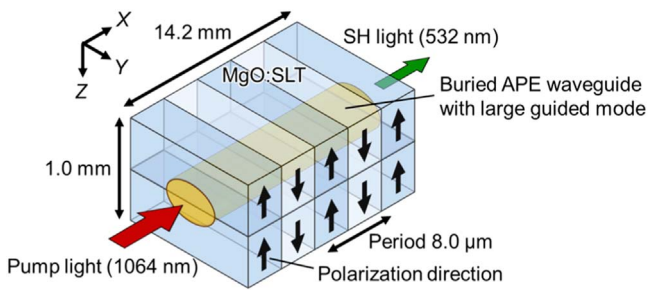

Fig. 1. Schematic of buried APE waveguide in PP MgO:SLT crystal.

waveguide is fabricated by PE on one of the two PP MgO:SLT crystals, followed by surface-activated bonding (SAB)[33,34] of them and annealing for proton diffusion. This buried APE waveguide has a symmetric refractive index profile for generating the SH light with a symmetric guided mode. If the PP structures of the upper and lower crystals are misaligned in the longitudinal direction with each other, the conversion efficiency becomes worse because the SH light is not generated from the region where the polarization directions of the upper and lower crystals are opposite with each other. To avoid this, a uniform PP structure was formed on one of the crystals, and eight sets of PP structures were prepared on the other crystal, in which each PP structure was shifted by 1.0 μm in the longitudinal direction. The misalignment in the longitudinal direction will be lower than 0.5 μm for one of the eight sets even without any special effort for the longitudinal direction alignment during the SAB process. In the misaligned region, the nonlinear optical coefficient is practically zero since the upper and lower crystals have opposite polarizations and the SH light is not generated. Given the period of the PP structure is Λ and the length of the misaligned region is a, the first order Fourier coefficient of the nonlinear optical coefficient, which is an effective nonlinear optical coefficient d_{eff} in the first order QPM,[35] is calculated to be $(2/\pi) \times \cos(a\pi/\Lambda) \times d_{33}$ as in the theory of QPM without misalignment. Therefore, the effective nonlinear optical coefficient will be kept higher than $(2/\pi) \times \cos(\pi/16) \times d_{33}$ when the period Λ is 8.0 μm and the length of the misaligned region a is shorter than 0.5 μm. Theoretical values of the nonlinear coupling coefficient κ and the normalized conversion efficiency η_{norm} will be estimated from the observed guided mode profiles of the pump and the SH light in the fabricated buried APE waveguide. With 10 W of a 1064 nm pump light, about 2 W of a 532 nm SH light is expected to be generated with a 10 mm long MgO:SLT SHG buried waveguide. The SH power of 2 W and the residual pump power of 8 W are expected to be large enough to generate 1 W class 355 nm light by SFG. In order to accept a high SH power of 2 W, the $1/e^2$ diameter of the guided mode should be larger than 16 μm, which is calculated using the photorefractive damage threshold of 2 MW cm^{-2}.[17] The mode size of the pump light is expected to be about 1.5–2.0 times larger than that of the SH light.[16] Therefore, the mode size of the pump light should be about 30 μm.

3. Diffusion coefficients of protons in MgO:SLT and guided mode profiles

In order to roughly estimate the process condition, the mode profiles of channel waveguides were simulated. In APE waveguides, the proton concentration determines the refractive index, and the proton concentration in both PE and annealing processes can be determined by solving the diffusion equation. Therefore, the diffusion coefficient was first determined by measuring the proton concentration of slab waveguides by SIMS. In the following, the coordinates corresponding to the X, Y, and Z axis of the crystal are x, y, and z, respectively. In the slab waveguides, the proton concentration profile C after the PE and the annealing process is given by solving the diffusion equation in one dimension:[36]

© 2024 The Japan Society of Applied Physics

$$\frac{\partial C}{\partial t} = \frac{\partial}{\partial z}\left(D\frac{\partial C}{\partial z}\right) \tag{1}$$

where D is a temperature-dependent diffusion coefficient. In the PE process, the proton diffusion coefficient is modeled to depend on the lithium concentration, where the proton diffusion coefficient drastically increases when the lithium concentration reaches the critical value.[37] The proton concentration after the PE process, which is given by solving Eq. (1) under this model, is well approximated by a rectangular shape.[37] The depth of the edge of the rectangular shape d_{PE} obeys a standard square root law,[26]

$$d_{PE} = 2\sqrt{D_{PE}t_{PE}}, \tag{2}$$

where D_{PE} is the diffusion coefficient at the PE temperature. The proton concentration profile of slab waveguides after the annealing $C_a(z)$ is well approximated by solving Eq. (1) under the condition where the protons are diffused into the deep region with d_{PE} and the proton diffusion coefficient is independent of the lithium concentration,[37]

$$C_a(z) = \frac{C_0}{2}\left[\mathrm{erf}\left(\frac{d_{PE}+z}{d_a}\right) + \mathrm{erf}\left(\frac{d_{PE}-z}{d_a}\right)\right], \tag{3}$$

where C_0 is the initial proton concentration before annealing, z is the depth from the crystal surface, and d_a is the $1/e^2$ depth of the proton concentration profile by the annealing. d_a also follows the standard square root law,

$$d_a = 2\sqrt{D_a t_a}, \tag{4}$$

where D_a is the diffusion coefficient at the annealing temperature.

To investigate D_{PE} and D_a, SIMS measurements were performed for three $+Z$-MgO:SLT crystals processed with PE and annealing at different annealing times. Before the process, the $+Z$-MgO:SLT crystals were cleaned by 1,1,2-trichloroethane and acetone. Then the crystals were soaked in a pure pyrophosphoric acid at 230 °C for 4 h to perform PE. Two of the crystals were put in a quartz tube in a flowing dry oxygen and the temperature was gradually increased by about 100 °C h^{-1} to 400 °C. The temperature was kept at 400 °C for 25 h to diffuse the protons in the crystals and gradually decreased to room temperature. One of the crystals was subsequently annealed again in the furnace at 400 °C for 25 h hence the total annealing time was to be 50 h.

Figure 2 shows the SIMS profiles of these samples. Without annealing, the proton concentration was almost constant from the surface to the depth of 0.85 μm and substantially dropped as shown in Fig. 2(a). Although the proton exchange depth d_{PE} of 0.85 μm was measured using one datum, the diffusion coefficient D_{PE} along the Z direction using the pure pyrophosphoric acid at 230 °C was estimated from Eq. (1) to be 0.045 $\mu m^2\,h^{-1}$. This value is smaller than the reported value of 0.08 $\mu m^2\,h^{-1}$ for the $+Z$-cut congruent $LiTaO_3$ (CLT) crystal processed under the same PE condition.[25] The difference can be explained by the fact that MgO doping reduces the diffusion coefficient, as reported for CLN; the diffusion coefficients in CLN and MgO:CLN crystals are 0.33 $\mu m^2\,h^{-1}$ and 0.2 $\mu m^2\,h^{-1}$, respectively.[25] The SIMS profiles of the protons after the annealing for 25 h and 50 h are shown in Figs. 2(b) and 2(c), respectively. Both profiles became graded profiles. The proton concentration was unexpectedly decreased from the crystal surface to the depth of 5 μm when the crystal was annealed for 50 h. The same phenomenon was observed in CLN.[38] The protons near the crystal surface could be released from the crystal into the atmosphere due to the annealing at high temperatures. The proton concentration profiles were fitted using Eq. (3), except for the data from the surface to the depth of 5 μm for the crystal with 50 h annealing. From the fitting results, the diffusion depths d_a

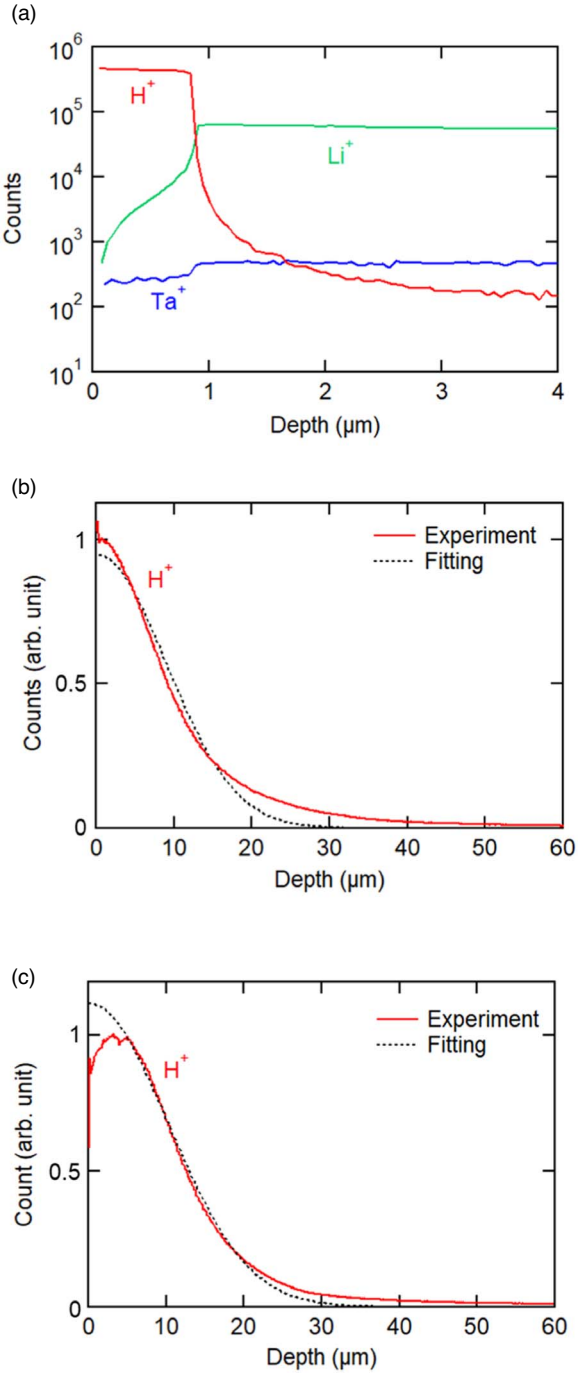

Fig. 2. (a) SIMS profiles in PE $+Z$-MgO:SLT crystal with PE temperature of 230 °C and PE time of 4 h. SIMS profiles in APE $+Z$-MgO:SLT crystal with PE temperature of 230 °C, PE time of 4 h, annealing temperature of 400 °C, and annealing time of (b) 25 h, and (c) 50 h (linear scale). Dotted lines in (b) and (c) are fitting curves of Eq. (3).

© 2024 The Japan Society of Applied Physics

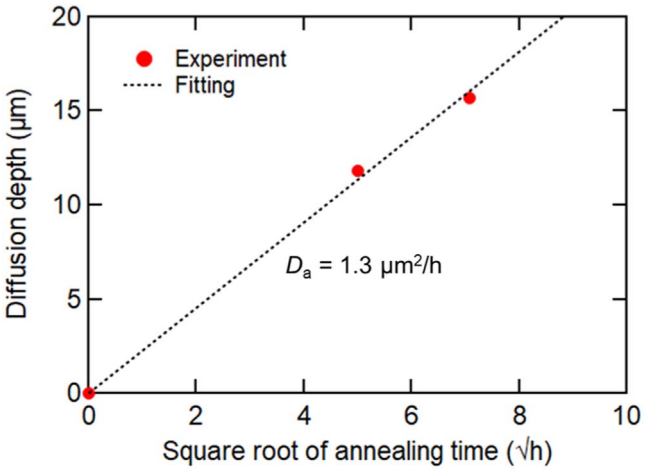

Fig. 3. Dependence of $1/e^2$ depth on square root of annealing time. Dotted line is fitting curve of Eq. (4).

of the annealing of 25 h and 50 h were estimated to be 11.8 μm and 17.9 μm, respectively. Figure 3 shows the diffusion depth d_a as a function of the square root of the annealing time. The data was fitted by Eq. (4), and the diffusion coefficient D_a along the Z direction for a temperature of 400 °C was estimated to be 1.3 $\mu m^2\,h^{-1}$, which was similar to that of MgO:SLT (0.9 $\mu m^2\,h^{-1}$) estimated by the mode size of the waveguide.[28)]

The refractive index profile of the buried APE waveguides was calculated using the estimated diffusion coefficients D_{PE} and D_a. The process was assumed to first perform the PE in a pure pyrophosphoric acid at 230 °C on a MgO:SLT crystal with a channel waveguide-shaped mask, followed by direct bonding with a non-PE MgO:SLT crystal and annealing at 400 °C. The proton concentration profile before the annealing is illustrated in Fig. 4(a). The proton concentration profile was a rectangular shape with a width of the PE width and a depth of d_{PE} estimated by Eq. (2). The surface of the PE region is protruded since the lattice constant of the PE region is larger than that of the original crystal.[39)] Thus, the air layer, whose thickness depends on the PE time, was inserted between the bonding interfaces except for the PE region. The 0.57% increase of the lattice constant in PE CLT is reported,[39)] and the increase of the lattice constant of PE MgO:SLT was assumed to be the same as that of CLT. In the channel waveguide, the proton concentration profile after the annealing was calculated by solving the diffusion equation in two dimensions:[36)]

$$\frac{\partial C}{\partial t} = \frac{\partial}{\partial y}\left(D_y \frac{\partial C}{\partial y}\right) + \frac{\partial}{\partial z}\left(D_z \frac{\partial C}{\partial z}\right) \tag{5}$$

where D_y and D_z are the diffusion coefficients along the Y and Z axes, respectively. Here, the diffusion coefficients along the Z axis was assumed to be the estimated diffusion coefficient D_a and the proton diffusion coefficients along the X and Y axes were assumed to be 1.5 times smaller than that along the Z axis due to the crystal anisotropy, as reported in CLT.[26)] In the calculation, the air layer was assumed to disappear by annealing as the lattice constant approached that of the original crystal. The diffusion coefficient in the region where the air layer originally existed was assumed to be 0 $\mu m^2\,h^{-1}$ since the crystals in this region were not atomically bonded.

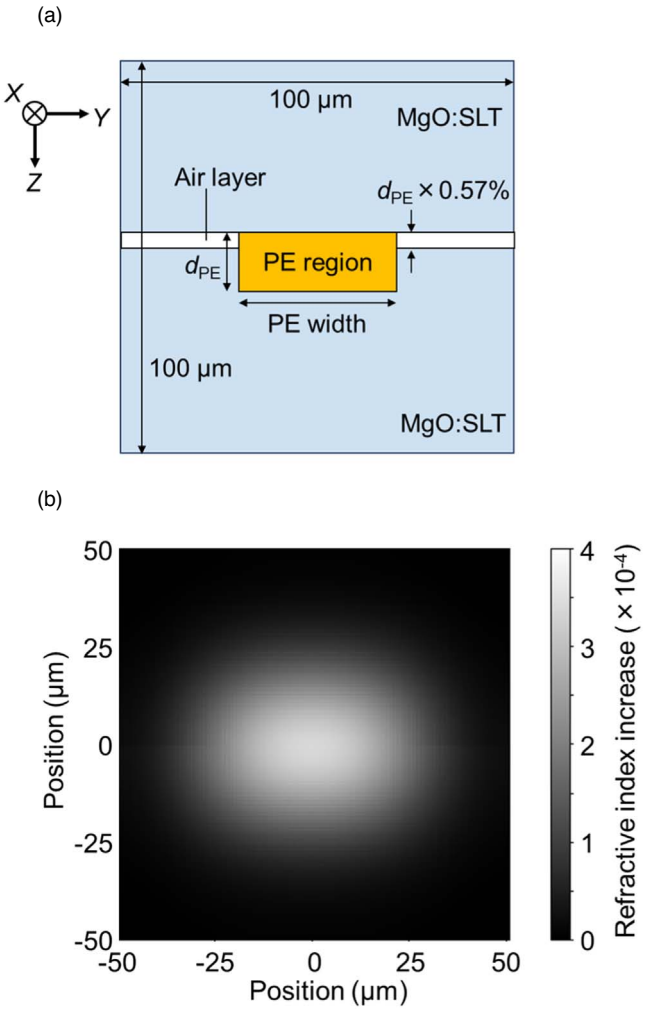

Fig. 4. (a) Model of proton concentration profile before annealing and (b) refractive index increase of waveguides with PE width of 50 μm, PE time of 8 h, and annealing time of 50 h.

After the proton concentration profile was estimated, the refractive index profile was calculated. The refractive index increase at the PE region Δn_0 was estimated to be 0.012 at 1030 nm wavelength, and the index increase Δn was expected to decrease in proportion to the proton concentration,[26,40)]

$$\Delta n = \Delta n_0 \frac{C}{C_0}. \tag{6}$$

Figure 4(b) shows the refractive index increase of the waveguide with a PE width of 50 μm, a PE time of 8 h, and an annealing time of 100 h. It was confirmed that the waveguide became a graded index waveguide due to the annealing. Using the calculated refractive index profile, the mode profiles of the channel waveguides were simulated using the mode solver based on finite-element methods (RSoft, FemSIM). The simulated mode profiles were fitted using the 2D Gaussian function and the $1/e^2$ diameters were calculated for the width and depth directions, respectively.

Figure 5 shows simulation results of the fundamental guided modes at a wavelength of 1030 nm of the buried APE waveguides. Red and blue lines represent $1/e^2$ diameters in the width and depth, respectively. As shown in Fig. 5(a), the mode diameters in the width increased in response to the

© 2024 The Japan Society of Applied Physics

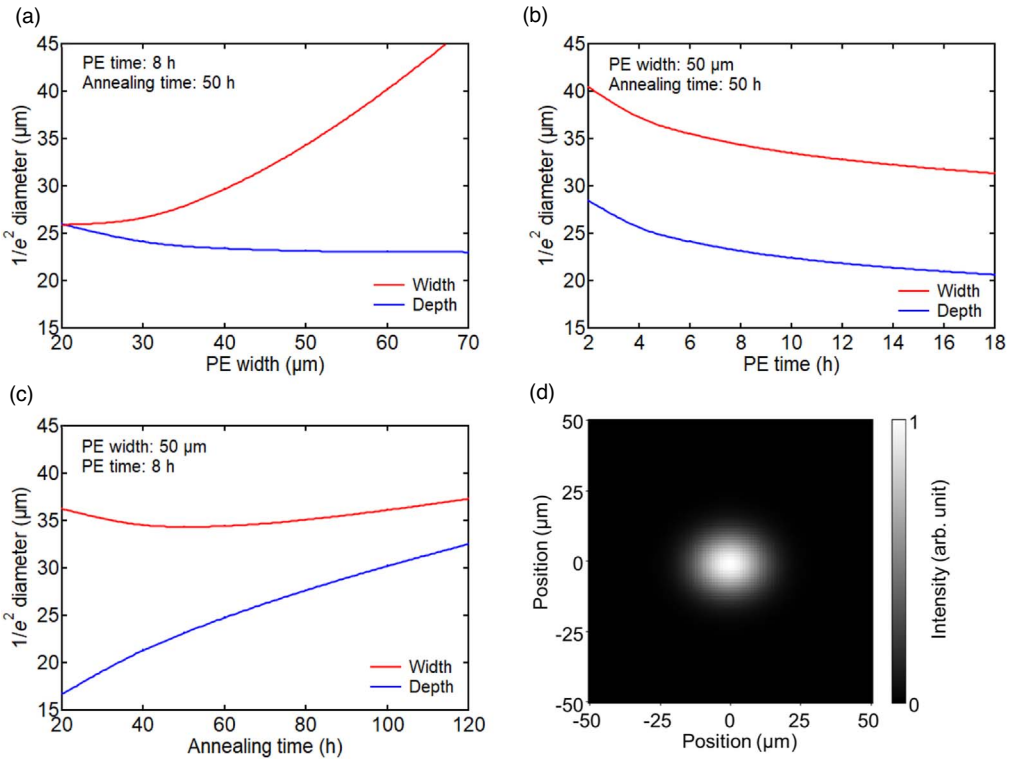

Fig. 5. Simulation results of fundamental guided modes of buried APE waveguides. Dependance of $1/e^2$ diameters on (a) PE width, (b) PE time, and (c) annealing time. (d) Guided mode profile of waveguide with PE width of 50 μm, PE time of 8 h, and annealing time of 100 h.

PE width. The mode diameters in the depth, on the other hand, decreased monotonously when the PE width increased since the waveguide confined the light strongly due to the larger intake amount of the protons. As shown in Fig. 5(b), the mode diameters increased when the total intake amount of the protons decreased due to the less PE time. When the annealing time was extended, the mode diameters increased as shown in Fig. 5(c) since the proton diffused more in the crystal. Waveguides with a $1/e^2$ diameter of more than 30 μm that could propagate the watt-class SH light were observed in several process conditions. Specifically, in the waveguide with a PE width of 50 μm, a PE time of 8 h, and an annealing time of 100 h, the $1/e^2$ diameters of the mode in the width and depth were 36 μm and 30 μm, respectively, as shown in Fig. 5(d). It could be confirmed that the guided mode had the Gaussian profile. The mode diameters in the width and depth of the 532 nm light in these waveguides were estimated to be 23 μm and 19 μm, respectively, where the refractive index increase at the PE region Δn_0 in Eq. (5) was assumed to be 0.017. The mode area for a wavelength of 532 nm was calculated to be 3.4×10^2 μm^2, and up to 3.4 W of the guided green light can be propagated to this waveguide, which was the value such that the maximum power density does not exceed the photorefractive damage threshold of MgO:SLT of 2 MW cm^{-2}.

4. Guided modes of buried APE waveguides

To confirm the simulated results and determine the process conditions of the waveguides, buried APE waveguides without the PP structures were fabricated. Figure 6 shows the fabrication process. (a) Ta masks with a thickness of 100 nm and target opening widths of 20 μm, 30 μm, 40 μm, 50 μm, and 60 μm were sputtered on the $+Z$ surface of the

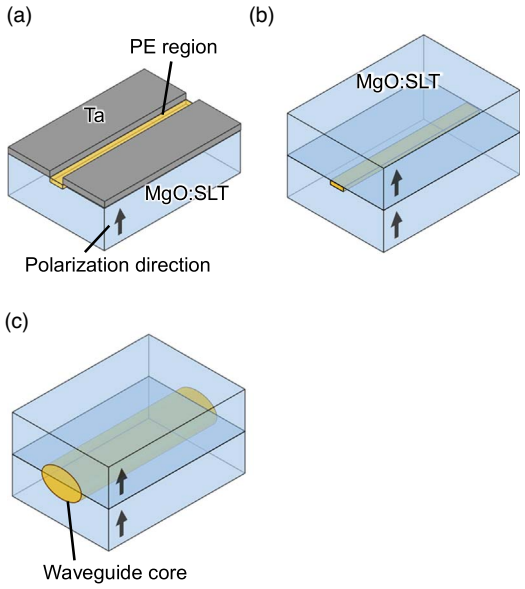

Fig. 6. Fabrication process of buried APE waveguides. (a) Ta mask sputtering and proton exchanging. (b) Ta mask removal and surface-activated bonding with non-PE MgO:SLT crystal. (c) Annealing for proton diffusion.

MgO:SLT crystals such that the waveguides were to be along with X-axis of the crystals. The actual opening widths were measured to be 18 μm, 28 μm, 38 μm, 48 μm, and 58 μm. PE was performed by soaking the crystals in pure pyrophosphoric acid at 230 °C for 4 h, 8 h, and 16 h to change the intake amounts of protons. The Ta masks were removed by $NaOH/H_2O_2$ solution. The surface morphologies were evaluated by the Nano 3D Optical Interferometry System (Hitachi, VS 1800). The PE regions protruded by approximately 7–9 nm, 7–10 nm, and 8–10 nm for 4 h, 8 h, and 16 h PE crystals, respectively. These protrusions are due to the

© 2024 The Japan Society of Applied Physics

extension of the lattice constant of the crystal due to the PE, as reported in CLT.[39] (b) The $-Z$ surface of MgO:SLT crystals and $+Z$ surface of the PE MgO:SLT crystals were cleaned by 1,1,2-trichloroethane and acetone. Both crystals were set in a chamber, and the chamber pressure was evacuated to be below 5×10^{-5} Pa. The surfaces were activated by an Ar fast atomic beam (FAB) with an FAB voltage of 1.0 kV and an FAB current of 200 mA for 100 s. Then, the surfaces of the $-Z$-MgO:SLT crystal and $+Z$ PE MgO:SLT crystal were affixed together with a load pressure of 10 MPa. To increase the bonding strength, the temperature was gradually increased to 110 °C over a period of 1.5 h. The temperature was kept for 1.5 h and gradually decreased below 30 °C over a period of 3.0 h. The total pressing time was 6.0 h. Both end facets were formed by dicing and polishing the crystals for input and output coupling of the light. The bonding was not peeled off after the dicing and polishing processes because there were more than twenty waveguides in one chip and PE regions with a width of about 1 mm at the edge of the chip. Moreover, the surfaces could be protruded, and spontaneously bonded in between the PE region in the SAB process.[41] (c) The annealing for proton diffusion was performed in a quartz furnace at 400 °C for 25 h in a flowing dry oxygen atmosphere.[16] By the annealing, the protons diffused across the bonding interface in the crystals, and the graded index waveguides with an ellipse shape were formed. Therefore, by performing SAB on the MgO:SLT and PE MgO:SLT and then annealing, waveguides with nearly symmetric modes could be fabricated without strict alignment in the SAB process. To observe near-field patterns (NFPs) of the guided modes, a CW laser light with a wavelength of 1032 nm and a $1/e^2$ diameter of 30 μm was coupled to the waveguides. After the observation, the annealing was performed in the furnace again for 25 h to enlarge the mode sizes. This additional annealing and the observation of the NFPs were repeated twice for 4 h PE crystals, three times for 8 h PE and 16 h PE crystals.

In some process conditions, the fundamental guided modes were observed. As shown in Fig. 7(a), the $1/e^2$ diameters of the guided mode in width and depth were 24 μm and 22 μm, respectively, in a waveguide with a PE width of 28 μm, a PE time of 8 h and an annealing time of 50 h. The guided modes were not observed in the waveguides with a PE width of 18 μm, though waveguides could be fabricated according to the simulation results. In this condition, the proton concentration was too small to provide optical confinement due to small intake amounts of protons. The higher order mode was propagated when the PE width was widened. This was because more protons were taken in the crystals and the waveguides confined the light more strongly. The waveguide with a PE width of 48 μm, a PE time of 4 h, and an annealing time of 50 h also had the guided mode with a $1/e^2$ diameter of 30 μm in width and 27 μm in depth, as shown in Fig. 7(b). When the PE time increased, the higher order modes were propagated since more protons were taken in the crystals. Figure 7(c) shows a NFP of the waveguide with a PE width of 48 μm, a PE time of 8 h, and an annealing time of 100 h. the $1/e^2$ diameters in the width and depth were 32 μm and 30 μm, respectively. The simulated mode diameters of the waveguide with a PE width of 48 μm, a PE time of 8 h, and an annealing time of 100 h were 36 μm and 30 μm, respectively. The measured mode diameters in the depth direction were in good agreement with the simulated ones. The measured mode diameters in the width direction, however, were smaller than the simulated ones. This discrepancy was expected to be attributed to the actual proton diffusion coefficient in the crystal Y-axis being smaller than the assumed one. Additionally, it is plausible that the air layer did not disappear by the annealing and acted as a cladding. In this case, however, the proton concentration profile was calculated to be almost the same as if the air layer disappeared except for the existence of the air layer. This was because the air layer was much thinner than the PE depth, and the diffusion coefficient in the region where the air layer originally existed was assumed to be 0 $\mu m^2\ h^{-1}$ in the calculation when the air layer disappeared. Therefore, the mode diameter in the width would decrease.

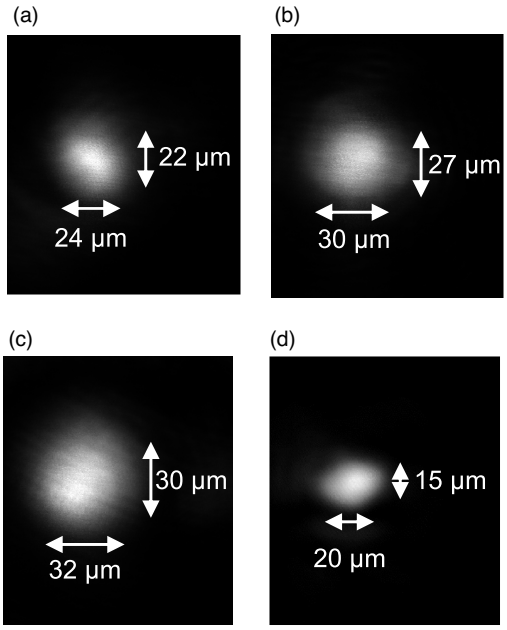

Fig. 7. NFPs with a wavelength of 1032 nm of fundamental guided modes of buried APE waveguides with (a) PE width of 28 μm, PE time of 8 h, and annealing time of 50 h, (b) PE width of 48 μm, PE width of 4 h, and annealing time of 50 h, and (c) PE width of 48 μm, PE time of 8 h, and annealing time of 100 h. (d) NFP of guided mode with a wavelength of 532 nm with PE width of 48 μm, PE time of 8 h, and annealing time of 100 h.

To investigate the mode size of the SH light, CW green laser light at a wavelength of 532 nm was directly coupled to the waveguide with a PE width of 48 μm, a PE time of 8 h, and an annealing time of 100 h, and NFP was observed. As shown in Fig. 7(d), the green-guided mode was almost symmetric as well as the IR-guided mode. The $1/e^2$ diameters in width and depth were 20 μm and 15 μm, respectively. The mode area was calculated to be $2.4 \times 10^2\ \mu m^2$, and up to 2.4 W of the guided light can be propagated to this waveguide.

5. Fabrication of SHG devices with buried APE waveguides

Figure 8 shows the fabrication process of the SHG device with the buried APE waveguide. 0.5 mm thick Z-cut 1.0 mol% MgO:SLT wafer was diced into $17.5 \times 9.0\ mm^2$ chips. (a) Periodic resist patterns with a period of 8.0 μm

© 2024 The Japan Society of Applied Physics

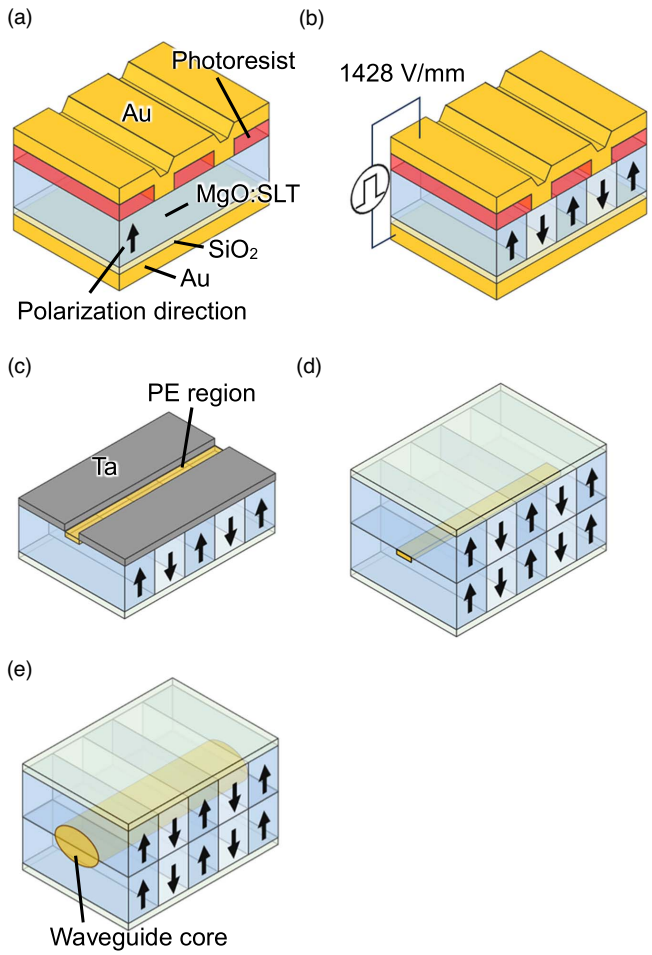

Fig. 8. Fabrication process of buried APE waveguide in PP MgO:SLT crystal. (a) Corrugated electrode formation. (b) Voltage application to form PP structures. (c) Proton exchange with Ta mask. (d) Surface-activated bonding. (e) Annealing for proton diffusion.

were formed by photolithography on the $+Z$ surface. Au with a thickness of 250 nm was evaporated on the $+Z$ surface to form a corrugated electrode. On the $-Z$ surface, a 1.0 μm thick SiO_2 insulation layer was sputtered to avoid a current leakage during the voltage application.[16] Then, a flat Au electrode was evaporated. (b) A pulsed electric field was applied to the crystal at 120 °C to form the PP structures. The electric field, the pulse width, and the pulse period were 1428 V mm^{-1}, 0.05 ms, and 0.15 ms, respectively. From the spontaneous polarization density of MgO:SLT $P_s = 55$ μC cm^{-2}[42] and the domain inversion area $S = 0.29$ cm^2, the domain inversion charge amount was calculated to $Q = 2P_sS = 32$ μC. After approximately 1500 pulses were applied, the charge amount supplied to the crystal reached 32 μC. The Au electrodes were removed by KI/I solution and the photoresist were removed by acetone. (c) A Ta mask with a thickness of 100 nm and an opening width of 48 μm was formed on the $+Z$ surface of one of the PP crystals by sputtering and lift-off process. PE was performed by soaking the crystal in a pure pyrophosphoric acid with a temperature of 230 °C for 8 h. The Ta mask was removed by a $NaOH/H_2O_2$ mixed solution. (d) After the two crystals were set in the vacuum chamber, the $+Z$ surface of both crystals was activated by Ar FAB with an FAB voltage of 1.0 kV and an FAB current of 200 mA for 100 s. The surfaces were affixed together with a load pressure of 10 MPa. To increase the bonding strength, the temperature was gradually increased to 110 °C over a period of 1.5 h. The temperature was kept for 1.5 h and gradually decreased below 30 °C over a period of 3.0 h. The total pressing time was 6.0 h. The bonding was made with a rotational misalignment of less than 0.04°. Both end facets of the waveguide were polished. The device length was measured to be 14.2 mm. (e) The annealing for proton diffusion was performed in a quartz furnace at 400 °C for 90 h in a flowing dry oxygen atmosphere. Here, the annealing time was reduced due to the difference in the wavelength for the NFP observation in Sect. 4 (1030 nm) and the pump light of the SHG experiment (1064 nm).

6. SHG experiments

SHG characteristics of the buried APE waveguide in PP MgO:SLT were evaluated using the CW laser with a wavelength of 1064 nm. The pump light polarized along the vertical direction was focused to a $1/e^2$ diameter of 39 μm and 29 μm in the horizontal and vertical direction, respectively, and coupled to the waveguide. The position of the device was aligned so that the pump light propagated as a fundamental mode, although the fabricated buried APE waveguide was a multimode waveguide. The output lights from the waveguide passed through a 20× objective lens and an imaging lens. An iris was installed at the focal position of the imaging lens to block the stray light. The powers of the pump light through a long pass filter with a cutoff wavelength of 700 nm and the SH light through a short pass filter with a cutoff wavelength of 550 nm were measured by a power meter. When the device temperature was changed using a Peltier stage with an accuracy of 0.1 °C, the SH light with a wavelength of 532 nm was generated, which was measured by a spectrometer. The device that generated maximum SH light power was selected. The pump and SH powers in the waveguide were estimated by taking the Fresnel reflections at the end facet of the device and the transmittance of the optical system into account. The reduction of the pump light in the waveguide due to the SHG and propagation loss was ignored. As shown in Fig. 9(a), the dependence of the η_{norm} value on the device temperature of 15.0 °C–35.0 °C with a pump power of approximately 400 mW was measured. The η_{norm} had a peak at the device temperature of 25.5 °C and the full-width at half-maximum (FWHM) was 2.5 °C. The theoretical values of the peak temperature and the FWHM of the bulk device were 31.5 °C and 2.3 °C, respectively, which were calculated using the refractive index of the bulk MgO:SLT crystal.[10] The difference in the peak temperatures implies that the PE increased the refractive index difference between the pump and the SH light since the refractive index difference increased with the temperature rise. From the result that the measured FWHM was almost the same as the theoretical value in the bulk device, the slope of the temperature dependence of the refractive index at the phase-matching wavelength was not almost changed by the PE. Figure 10 shows the NFPs of the guided modes of the pump and SH lights at a device temperature of 25.5 °C. The pump and SH lights propagated with the fundamental modes. Although the shapes were slightly longer at the bottom, they were almost symmetric. The $1/e^2$ diameters in the width and depth were 31 μm and 31 μm for the pump light and 19 μm

© 2024 The Japan Society of Applied Physics

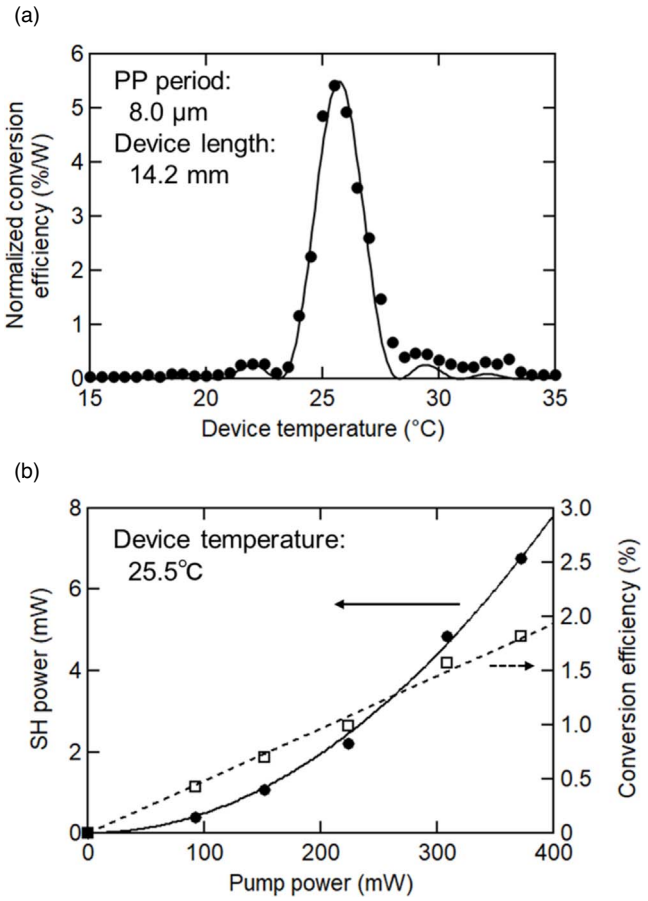

Fig. 9. SHG characteristics. (a) Dependence of normalized conversion efficiency on device temperature and (b) dependence of SH power and conversion efficiency on pump power at a device temperature of 25.5 °C.

and 16 μm for the SH light, respectively. From the guided modes of both pump and SH lights, the nonlinear coupling coefficient was calculated back to be 0.16 $W^{-1/2}\,cm^{-1}$.

Figure 9(b) shows the dependence of the SH power and conversion efficiency on the pump power at a device temperature of 25.5 °C. The SH power was proportional to the square of the pump power, and a maximum SH power of 6.7 mW was obtained. The η_{norm} was estimated to be 4.8% W^{-1}, corresponding to a nonlinear coupling coefficient of 0.15 $W^{-1/2}\,cm^{-1}$. This nonlinear coupling coefficient was close to that calculated by the guided modes. Although the guided mode diameter was comparable to the beam waist in bulk devices, the higher conversion efficiency can be obtained in the buried APE waveguide devices since the guided mode size is maintained throughout the full length of the waveguides. Considering the nonlinear coupling coefficient of 0.15 $W^{-1/2}\,cm^{-1}$, the 2 W SH light is expected to be generated from a 10 mm long device with 10 W pumping. Considering that the comparable nonlinear coupling coefficient of 0.15 $W^{-1/2}\,cm^{-1}$ for our previously-reported asymmetric APE waveguide,[16] the SHG with a symmetric guided mode was successfully demonstrated while maintaining the nonlinear coupling coefficient, which is suitable for high-resolution industrial applications. Moreover, the waveguide with a large guided mode can be used for mid-infrared optical devices.

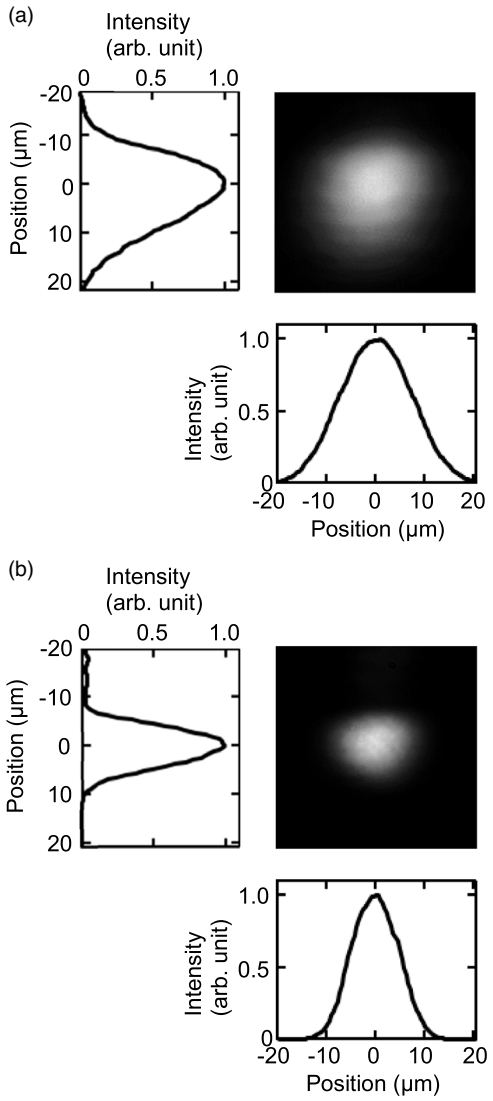

Fig. 10. NFPs and intensities of guided modes of (a) pump light and (b) SH light at a device temperature of 25.5 °C.

7. Conclusions

The SIMS analysis revealed that the diffusion coefficient of the protons in MgO:SLT of the PE with a pure pyrophosphoric acid at 230 °C was 0.045 $\mu m^2\,h^{-1}$ and smaller than that of CLT. The diffusion coefficient of the annealing at 400 °C was 1.3 $\mu m^2\,h^{-1}$. The buried APE waveguides were fabricated using the process with the order of the PE, the SAB, and the annealing. The waveguides exhibited the symmetric guided mode profile. Specifically, the buried APE waveguides with $1/e^2$ diameters of 32 μm in width and 30 μm in depth at a wavelength of 1030 nm were fabricated with a PE width of 48 μm, a PE time of 8 h, and an annealing time of 100 h. The guided mode at a wavelength of 532 nm in this waveguide was also symmetric with $1/e^2$ diameters of 20 μm in the width and 15 μm in the depth. The buried waveguides in PP MgO:SLT were fabricated by SAB for high-power SHG with a pump light of 1064 nm. The SHG was performed with a pump power of about 400 mW. The $1/e^2$ diameters in width and depth were 31 μm and 31 μm for the pump light and 19 μm and 16 μm for the SH light,

© 2024 The Japan Society of Applied Physics

respectively. The nonlinear coupling coefficient was estimated to be 0.15 $W^{-1/2}$ cm^{-1}. The 2 W SH light is expected to be generated from a 10 mm long device with 10 W pumping. Compared to the conventional APE waveguide SHG device without SAB, the guided mode of the pump and SH light were symmetric, which is suitable for high-resolution industrial applications.

Acknowledgments

This work was partly supported by Osaka University Fellowship "Quantum Leader Resources" (QLEAR Fellowship) and Spintronics Research Network Division, Institute for Open and Transdisciplinary Research Initiatives, Osaka University. We acknowledge the support of the Photonics Center, Osaka University. We acknowledge the use of Optical Interferometry System was supported by Prof. Yusuke Mori and Prof. Masayuki Imanishi, Osaka University.

ORCID iDs

Tomoyuki Tanikawa https://orcid.org/0000-0003-0148-9701

1) X. Ya, Q. Liu, M. Gong, X. Fu, and D. Wang, Appl. Phys. B **95**, 323 (2009).
2) X. Yan, Q. Liu, H. Chen, X. Fu, M. Gong, and D. Wang, Laser Phys. Lett. **7**, 563 (2010).
3) M. Yoshimura, K. Murase, T. Kamimura, K. Nakai, Y. K. Yap, Y. Mori, T. Sasaki, Y. Matsumoto, and Y. Okada "Advanced solid state lasers," *OSA Trends in Optics and Photonics*, ed. M. Fejer et al., (Optica Publishing Group, Boston, 1999)Vol. 26, p. 112.
4) Y. C. Wu, F. Chang, P. Z. Fu, C. T. Chen, G. L. Wang, A. C. Geng, Y. Bo, D. F. Cui, and Z. Y. Xu, "High-Average-Power Third Harmonic Generation at 355 nm with CsB3O5 Crystal," Chinese Phys. Lett. **22**, 1426 (2005).
5) Z. Lin, L. F. Xu, R. K. Li, Z. Wang, C. Chen, M. H. Lee, E. G. Wang, and D. S. Wang, Phys. Rev. B **70**, 233104 (2004).
6) I. Shoji, T. Kondo, A. Kitamoto, M. Shirane, and R. Ito, J. Opt. Soc. Am. B **14**, 2268 (1997).
7) D. S. Hum, R. K. Route, G. D. Miller, V. Kondilenko, A. Alexandrovski, J. Huang, K. Urbanek, R. L. Byer, and M. M. Fejer, J. Appl. Phys. **101**, 093108 (2007).
8) S. V. Tovstonog, S. Kurimura, I. Suzuki, K. Takeno, S. Moriwaki, N. Ohmae, N. Mio, and T. Katagai, Opt. Express **16**, 11294 (2008).
9) S. Sinha, D. S. Hum, K. E. Urbanek, Y. W. Lee, M. J.-F. Digonnet, M. M. Fejer, and R. L. Byer, J. Light. Technol. **26**, 3866 (2008).
10) I. Dolev, A. Ganany-Padowicz, O. Gayer, A. Arie, J. Mangin, and G. Gadret, Appl. Phys. B **96**, 423 (2009).
11) H. H. Lim, T. Katagai, S. Kurimura, T. Shimizu, K. Noguchi, N. Ohmae, N. Mio, and I. Shoji, Opt. Express **19**, 22588 (2011).
12) J. Hirohashi, Y. Tomihari, T. Fukui, S. Makio, K. Suzuki, K. Imai, H. Motegi, and Y. Furukawa, *Lasers, Sources, and Related Photonic Devices, OSA Technical Digest (CD)* (Optica Publishing Group, San Diego, 2012), paper AT4A.22.
13) J. Sun and C. Xu, Opt. Lett. **37**, 2028 (2012).
14) H. H. Lim, S. Kurimura, K. Noguchi, and I. Shoji, Opt. Express **22**, 18268 (2014).
15) A. A. Surin, T. E. Borisenko, and S. V. Larin, Opt. Lett. **41**, 2644 (2016).
16) R. Noro, M. Okazaki, I. Mizobata, M. Uemukai, T. Tanikawa, and R. Katayama, Jpn. J. Appl. Phys. **61**, 072006 (2022).
17) Y. Furukawa, M. Nakamura, S. Takekawa, K. Kitamura, T. Hatanaka, K. Nakamura, H. Ito, A. Alexandrovski, and M. M. Fejer, in *Advanced Solid-State Lasers*, ed. C. Marshall, (Optica Publishing Group, Seattle, 2001) Vol. 50, p. 685.
18) Y. Furukawa, K. Kitamura, A. Alexandrovski, R. K. Route, M. M. Fejer, and G. Foulon, Appl. Phys. Lett. **78**, 1970 (2001).
19) S. Enomoto and S. Ashihara, J. Appl. Phys. **110**, 063111 (2011).
20) A. Bruner, D. Eger, and S. Ruschin, J. Appl. Phys. **96**, 7445 (2004).
21) T. Umeki, O. Tadanaga, and M. Asobe, IEEE J. Quantum Electron. **46**, 1206 (2010).
22) R. Kou, S. Kurimura, K. Kikuchi, A. Terasaki, H. Nakajima, K. Kondou, and J. Ichikawa, Opt. Express **19**, 11867 (2011).
23) M. Chauvet, F. Henrot, F. Bassignot, F. Devaux, L. Gauthier-Manuel, V. Pecheur, H. Maillotte, and B. Dahmani, J. Opt. **18**, 085503 (2016).
24) W. B. Spillman, N. A. Sanford, and R. A. Soref, Opt. Lett. **8**, 497 (1983).
25) K. Yamamoto, K. Mizuuchi, and T. Taniuchi, Jpn. J. Appl. Phys. **31**, 1059 (1992).
26) P. J. Matthews, A. R. Mickelson, and S. W. Novak, J. Appl. Phys. **72**, 2562 (1992).
27) G. M. Davis and N. A. Lindop, J. Appl. Phys. **77**, 6121 (1995).
28) M. Okazaki, T. Chichibu, S. Yoshimoto, H. Mizuno, and T. Suhara, Jpn. J. Appl. Phys. **54**, 070301 (2015).
29) K. R. Parameswaran, R. K. Route, J. R. Kurz, R. V. Roussev, M. M. Fejer, and M. Fujimura, Opt. Lett. **27**, 179 (2002).
30) M. Marangoni, R. Osellame, R. Ramponi, S. Takekawa, M. Nakamura, and K. Kitamura, Opt. Express **12**, 2754 (2004).
31) M. Marangoni, M. Lobino, R. Ramponi, E. Cianci, and V. Foglietti, Opt. Express **14**, 248 (2006).
32) M. Fujimura, K. Beniya, and T. Suhara, Electron. Lett. **44**, 856 (2008).
33) H. Takagi, K. Kikuchi, R. Maeda, T. R. Chung, and T. Suga, Appl. Phys. Lett. **68**, 2222 (1996).
34) H. Takagi, J. Utsumi, M. Takahashi, and R. Maeda, ECS Trans. **16**, 531 (2008).
35) T. Suhara and M. Fujimura, *Waveguide Nonlinear-Optic Devices* (Springer, Berlin, 2003), Chap. 3.
36) J. Crank, *The Mathematics of Diffusion* (Oxford University Press, London, 1975) 2nd ed. Chap. 7.
37) S. T. Vohra, A. R. Mickelson, and S. E. Asher, J. Appl. Phys. **66**, 5161 (1989).
38) J. M. Zavada, H. C. Casey Jr, R. J. States, S. W. Novak, and A. Loni, J. Appl. Phys. **77**, 2697 (1995).
39) T. Yuhara, K. Tada, and Y. S. Li, J. Appl. Phys. **71**, 3966 (1992).
40) T. Suhara and M. Fujimura, *Waveguide Nonlinear-Optic Devices* (Springer, Berlin, 2003), Chap. 6.
41) H. Takagi, R. Maeda, T. Chung, N. Hosoda, and T. Suga, Jpn. J. Appl. Phys. **37**, 4197 (1998).
42) K. Kitamura, Y. Furukawa, K. Niwa, V. Gopalan, and T. E. Mitchell, Appl. Phys. Lett. **73**, 3073 (1998).

© 2024 The Japan Society of Applied Physics